nature cell biology

Adaptive braking by Ase1 prevents overlapping microtubules from sliding completely apart

Marcus Braun[1,2,4], Zdenek Lansky[3,4], Gero Fink[1,2,4], Felix Ruhnow[1,2], Stefan Diez[1,2,5] and Marcel E. Janson[3,5]

Short regions of overlap between ends of antiparallel microtubules are central elements within bipolar microtubule arrays. Although their formation requires motors[1], recent *in vitro* studies demonstrated that stable overlaps cannot be generated by molecular motors alone. Motors either slide microtubules along each other until complete separation[2–4] or, in the presence of opposing motors, generate oscillatory movements[5–7]. Here, we show that Ase1, a member of the conserved MAP65/PRC1 family of microtubule-bundling proteins, enables the formation of stable antiparallel overlaps through adaptive braking of Kinesin-14-driven microtubule–microtubule sliding. As overlapping microtubules start to slide apart, Ase1 molecules become compacted in the shrinking overlap and the sliding velocity gradually decreases in a dose-dependent manner. Compaction is driven by moving microtubule ends that act as barriers to Ase1 diffusion. Quantitative modelling showed that the molecular off-rate of Ase1 is sufficiently low to enable persistent overlap stabilization over tens of minutes. The finding of adaptive braking demonstrates that sliding can be slowed down locally to stabilize overlaps at the centre of bipolar arrays, whereas sliding proceeds elsewhere to enable network self-organization.

Microtubule network assembly and maintenance requires the function of motor and non-motor proteins with microtubule crosslinking activity[8–10]. Important building blocks within networks are antiparallel microtubule overlaps as found in mitotic and meiotic spindles. There, microtubule ends emanating from opposite spindle poles are linked by kinesin motors forming the spindle midzone. As crosslinking motors actively slide microtubules relative to each other, regulation of microtubule–microtubule sliding (henceforth denoted as 'microtubule sliding') is needed to prolong the coupling of microtubules and maintain spindle integrity. The Ase1/PRC1/MAP65 protein family is of prime interest because its members passively crosslink antiparallel microtubules with high affinity[11–14]. How the activity of passive crosslinkers is coordinated with active motors to enable the formation of stable overlaps is unknown.

We describe an *in vitro* assay to study the role of *Schizosaccharomyces pombe* Ase1 (anaphase spindle elongation protein 1) as a regulator of microtubule sliding. To induce sliding, we used minus-end-directed *Drosophila* Kinesin-14, Ncd, which slides antiparallel microtubules[3]. In contrast to plus-end-directed motors Kinesin-5 and Kinesin-6, Ncd is unlikely to interact biochemically with Ase1, allowing us to focus on physical aspects of regulation[15,16]. We found that Ase1 slowed down motorized microtubule sliding in a dose-dependent manner. When microtubules started to slide apart, Ase1 density increased in overlaps, leading to an amplified slowdown. Feedback between density and velocity constitutes an adaptive braking system that prevents full separation of antiparallel microtubules.

To investigate the influence of Ase1 crosslinkers on motorized microtubule sliding we imaged Ncd-induced, antiparallel sliding of 'transport' microtubules along long surface-immobilized 'template' microtubules[3] (Fig. 1a). Keeping the Ncd concentration constant, we added green fluorescent protein (GFP)-tagged Ase1 and observed a progressive slowdown of transport microtubules as Ase1–GFP accumulated strongly in the moving overlaps (Fig. 1b,c and Supplementary Movie S1). The sliding velocity and Ase1–GFP intensity reached steady state after approximately 5 min (Fig. 1e). We repeated the experiment using GFP–Ncd and unlabelled Ase1 and did not observe a strong accumulation of motors in overlaps (Fig. 1d). Furthermore, we confirmed that GFP–Ncd levels in overlaps were comparable before (48.9 ± 8.5 AU μm^{-1}, $\pm$s.e.m., $n = 12$) and after (60.4 ± 14 AU μm^{-1}, $\pm$s.e.m., $n = 8$) the addition of Ase1 (0.39 nM). We conclude that Ase1 binding slowed down motorized sliding but did not displace Ncd from overlaps. This explains the progressive slowdown of elongating microtubules within microtubule bundles of *S. pombe* cells. There, the ratio between bound motors and Ase1 decreases during elongation[9].

[1]Max Planck Institute of Molecular Cell Biology and Genetics, Pfotenhauerstraße 108, 01307 Dresden, Germany. [2]B CUBE, Technische Universität Dresden, Arnoldstr. 18, 01307 Dresden, Germany. [3]Laboratory of Plant Cell Biology, Wageningen University, Droevendaalsesteeg, 6708 PB Wageningen, The Netherlands. [4]These authors contributed equally to this work.
[5]Correspondence should be addressed to S.D. or M.E.J. (e-mail: diez@bcube-dresden.de or marcel.janson@wur.nl)

Received 8 March 2011; accepted 20 July 2011; published online 4 September 2011; DOI: 10.1038/ncb2323

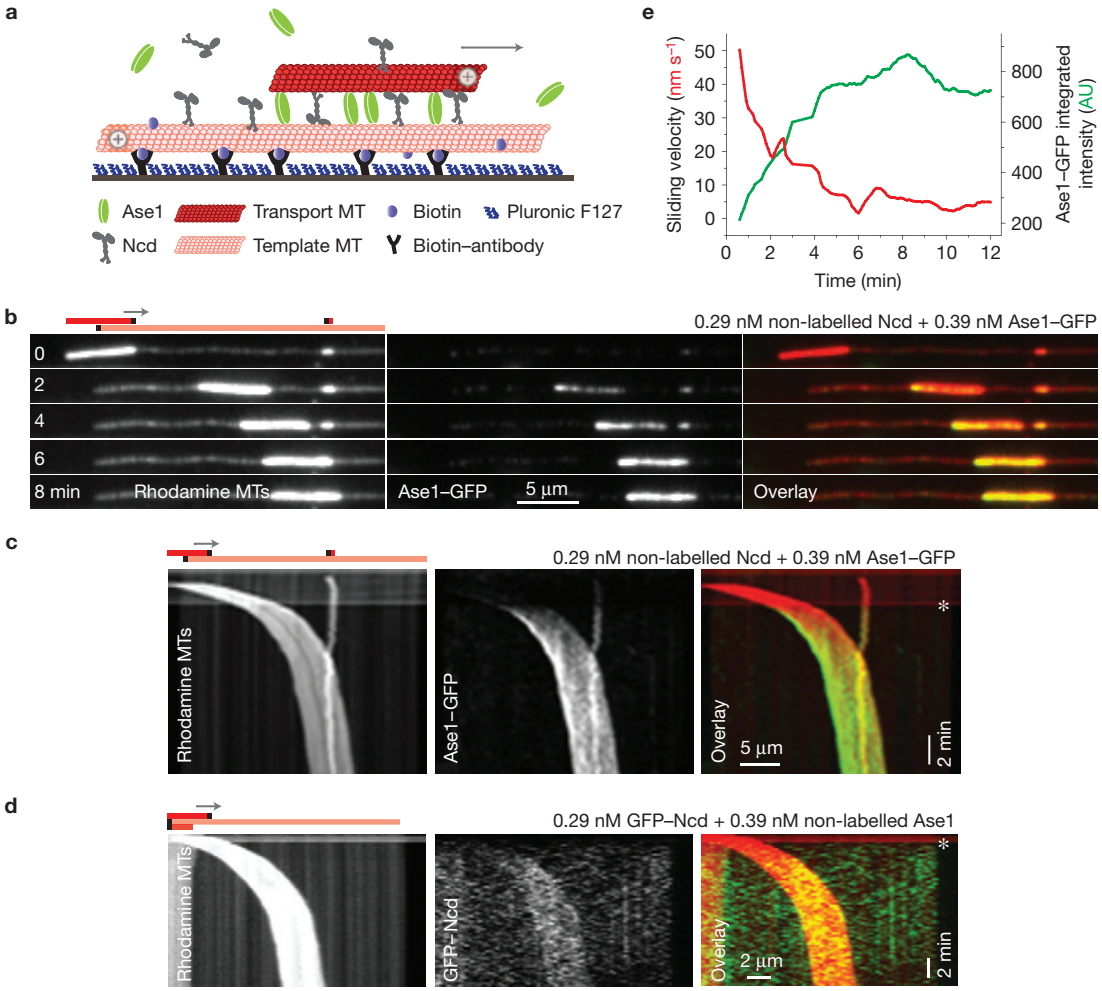

Figure 1 Ase1 slows Ncd-driven microtubule sliding. (**a**) Schematic representation of Ncd-driven sliding of a transport microtubule (MT) along a surface-immobilized template microtubule in the presence of Ase1. (**b**) Time-lapse fluorescence micrographs of transport microtubule motion before and after the addition of 0.39 nM Ase1–GFP at $t = 1.2$ min (the Ncd concentration is kept constant at 0.29 nM). The short transport microtubule on the right presumably has a parallel orientation and therefore is not moved by Ncd (ref. 3). The schematic diagram illustrates microtubule orientations and positions at the start of the experiment (template microtubule is dim red and transport microtubules are bright red; black marks indicate plus-ends). (**c**) Multi-channel kymographs of the experiment shown in **b**; the asterisk denotes the addition of Ase1–GFP. (**d**) Multi-channel kymographs of microtubule sliding with GFP–Ncd and non-labelled Ase1. (**e**) Quantification of transport microtubule sliding velocity and Ase1–GFP intensity in the overlap of the experiment in **b** and **c**.

Previous work on purified Eg5 and Ncd motors showed that transport microtubules continue to slide along template microtubules with constant velocity until their ends fully separate or become loosely tethered[3,4]. In contrast, in the presence of Ase1–GFP, we found that transport microtubules that initially moved steadily towards the minus-ends of template microtubules slowed down markedly when microtubules started to slide apart (Fig. 2a and Supplementary Movie S2). Strikingly, in all analysed events ($n = 48$), microtubules never separated during the course of our observation times (up to 1 h) but formed persistent antiparallel overlaps (Supplementary Fig. S1a) that lasted up to 1 h. During slowdown, when the overlap shortened, the density of Ase1–GFP (the fluorescence intensity per unit overlap length) progressively increased (Fig. 2b). In the absence of sliding, a similar correlation between Ase1–GFP density and overlap length was not observed (Supplementary Fig. S2a). Ase1–GFP often accumulated at the trailing ends of moving overlaps (Figs 1b,c and 2c, left panel). When microtubules started to slide apart Ase1–GFP accumulated at both ends of the overlap (Fig. 2c, right panel). Similar observations were obtained using the *S. pombe* Kinesin-14 Klp2 instead of Ncd (Supplementary Fig. S1b,c). These experiments demonstrate that Ase1–GFP does not leave the shrinking overlap but is retained therein and becomes compacted by converging microtubule ends independent of the cause of sliding. In contrast, we did not observe any redistribution or increase in density of GFP–Ncd in shrinking overlaps (Fig. 2d).

To explain the sliding-induced redistribution of Ase1–GFP in overlaps, we imaged Ase1–GFP at single-molecule levels. Ase1 exhibits fast one-dimensional diffusion along single microtubules and slower diffusion within microtubule overlaps[17]. At low Ase1–GFP concentration, before the addition of Ncd, we observed diffusion of transport microtubules in addition to diffusion of Ase1–GFP (Fig. 3a). This demonstrated that low Ase1 numbers hardly hinder lateral motion of crosslinked microtubules. After the addition of Ncd, Ase1–GFP diffusion within overlaps continued but sliding induced an additional

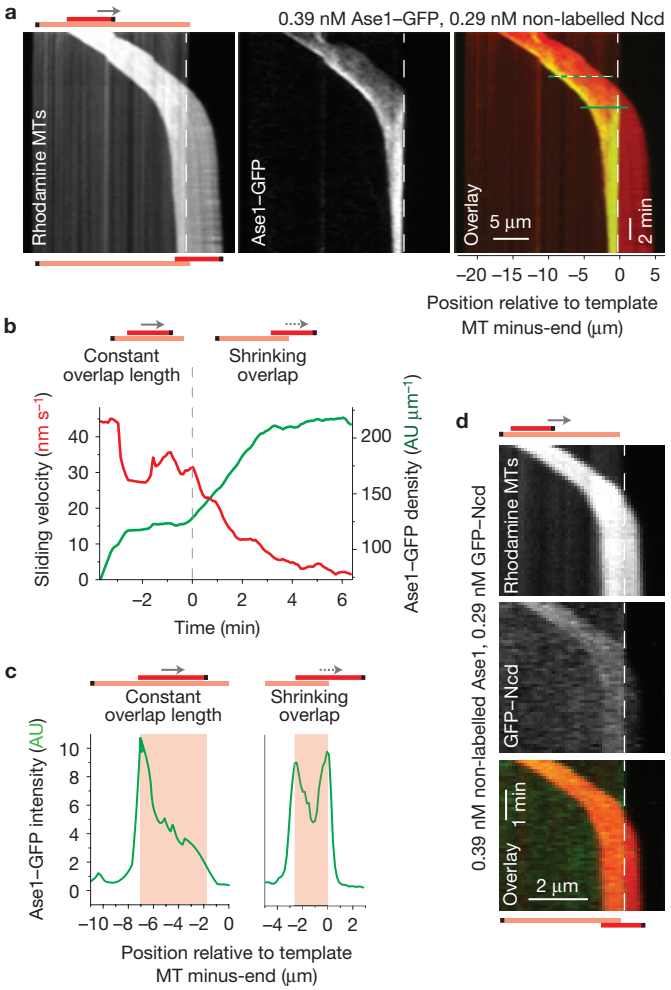

Figure 2 Ase1 prevents antiparallel microtubules from sliding completely apart. (**a**) Typical multi-channel kymographs showing the slowdown of microtubule (MT) sliding, as well as the distribution of Ase1–GFP, when a transport microtubule starts to slide apart from the template microtubule. The dashed lines indicate the position of the template microtubule minus-end. (**b**) Ase1–GFP density (right axis) and velocity of the transport microtubule (left axis) before and during overlap shrinkage. The dashed line indicates the start of separation. The brief slowdown around −3 min coincides with the crossing of an additional template microtubule (Supplementary Movie S2). (**c**) Ase1–GFP profiles along the dashed (before the start of microtubule separation, left panel) and the solid green line (during microtubule separation, right panel) in **a**. (**d**) Typical multi-channel kymographs showing the GFP–Ncd distribution during slowdown of microtubule sliding.

drift of Ase1–GFP molecules at approximately half the sliding velocity (Fig. 3b, dashed arrow). Consequently, a net flux of Ase1–GFP was generated towards the trailing ends of transport microtubules. Remarkably, Ase1–GFP molecules tracked the trailing ends and did not leave the overlaps (Fig. 3b, arrowheads). In the absence of sliding, end-accumulation of Ase1–GFP was never observed[17]. We refer to sliding-induced end-tracking as 'molecular sweeping' and attribute it to the higher affinity by which Ase1 binds to microtubule overlaps in comparison with single microtubules[17]. Moving microtubule ends therefore form a barrier to Ase1 diffusion reminiscent of Dam1 and Ndc80 tracking on depolymerizing microtubule ends[18,19]. The combined effects of diffusion, drift and diffusion barriers redistribute Ase1 along the microtubule overlap following an exponential profile as suggested for convection–diffusion systems[20]. Accordingly, Ase1 profiles were steepest on fast-moving microtubules and flattened as microtubules slowed down (Supplementary Fig. S3). Sweeping occurs at both ends of shortening overlaps and therefore provides a molecular explanation for the compaction of Ase1 (Fig. 2a).

Any Ase1 compaction in shrinking overlaps above the equilibrium density will decay at the molecular off-rate. To determine whether this scheme explains the formation of stable antiparallel overlaps, we developed a model (Methods and Supplementary Table S1) that predicts the time evolution of overlap length, L, and the number of Ase1 crosslinkers in the overlap, n, from the conditions at time $t_0 = 0$, the moment that the microtubules start to slide apart. n is proportional to the integrated pixel intensity along the overlap written out in arbitrary units. To implement our model we analysed the relation between measured sliding velocities (v), Ase1–GFP signals and transport microtubule lengths using sliding data as in Fig. 1. Under constant Ncd densities, v decreased linearly with the measured Ase1–GFP density along transport microtubules (Fig. 4a) and did not correlate well with microtubule length (Supplementary Fig. S2b). Therefore, we assumed in our model that the velocity is a linear function of the Ase1–GFP density in the overlap (Fig. 4a). Accordingly, sliding is halted above a stopping density $\rho_{stop} = 229\ \mathrm{AU\,\mu m^{-1}}$ (intercept of linear fit with density axis). We estimate that this value corresponds to about one Ase1–GFP dimer per 50 nm overlap (Supplementary Fig. S4 and Movie S3).

In our model, the number of Ase1 crosslinkers in a shrinking overlap is determined by sweeping and molecular turnover, $\mathrm{d}n/\mathrm{d}t = n/L(1-\varepsilon)\mathrm{d}L/\mathrm{d}t + k_{on}L - k_{off}n$. The first term represents molecular sweeping with an efficiency ε ranging between 0 in the absence of sweeping and 1 in the case of complete retainment of Ase1 in overlaps. The second and third term represent Ase1 turnover in the microtubule overlap; k_{on} is the molecular on-rate ($\mathrm{AU\,s^{-1}\mu m^{-1}}$) and k_{off} is the off-rate ($\mathrm{s^{-1}}$). A sweeping efficiency of 0.72 ± 0.06 ($\pm$s.e.m.) was determined by analysing the observed increase in Ase1–GFP density as a function of overlap length after the initiation of overlap shrinkage (Fig. 4b and Methods). Photobleaching experiments on Ase1–GFP in overlaps yielded a fluorescence recovery time $1/k_{off} = 590 \pm 57$ s ($\pm$s.e.m.; Supplementary Fig. S5a).

Model predictions for overlap shrinkage were in excellent agreement with experimental data (Fig. 4c and Supplementary Movie S4). We modelled all events (9 out of 48 total events) for which the Ase1 density and sliding velocity reached equilibrium values before the transport microtubule reached the template end (Fig. 4d, Supplementary Fig. S5b and Methods). In these cases, k_{on} can be calculated from k_{off} and the steady-state Ase1–GFP density for each individual event. Taking v_0 and L_0 as input, the model predicts for the whole duration of the experiment without any fitting, first, the rate at which molecular sweeping during overlap shrinkage pushes the Ase1 density towards ρ_{stop} and, second, the resulting overlap length (subscript 0 indicates a parameter value at t_0). Overlap length predictions were accurate for seven events that varied over a wide range of transport microtubule lengths and v_0. In two remaining cases, the model deviated from the observed length, indicating that fluctuations in protein densities and transient non-specific surface interactions of the transport microtubules may be additional experimental factors that are unaccounted for in the model.

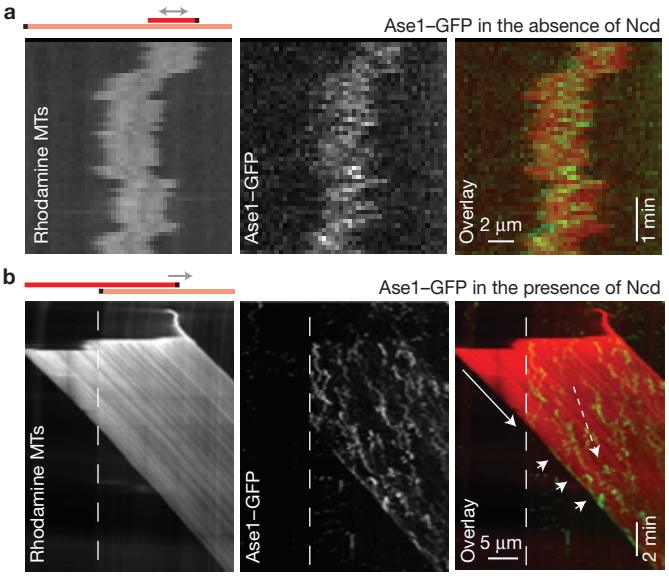

Figure 3 Moving microtubule ends constitute barriers for Ase1 diffusion. (**a**) One-dimensional diffusion of a transport microtubule (MT) relative to an immobilized template microtubule at low Ase1–GFP concentration. (**b**) Diffusion of single Ase1–GFP molecules within a moving microtubule overlap. The solid arrow shows the sliding velocity of the transport microtubule, the dashed arrow shows Ase1–GFP drift and the arrowheads show Ase1–GFP tracking to the trailing end of the microtubule overlap. The plus-end of the template microtubule is indicated by the dashed lines.

Our model explains a general trend in the data: transport microtubules arriving at the template ends with high Ase1 densities, ρ_0, have a low initial velocity, v_0, and only little Ase1 compaction is required to bring overlap shrinkage to a near halt (Fig. 4d). In contrast, microtubules that arrive with low ρ_0 and high v_0 show a large decrease in overlap length before Ase1 is compacted sufficiently to stabilize overlap length. This trend was also observed for microtubules that had not yet reached equilibrium Ase1 densities when overlap shrinkage started (23 additional events, black circles in Fig. 4e; Methods). Thus, Ase1 does not only allow for the formation of stable overlaps, but the actual Ase1 density ρ_0 also sets the resulting relative lengths of overlaps. We conclude that molecular sweeping and slow Ase1 turnover are sufficient to explain the prolonged stabilization of antiparallel microtubule overlaps in the presence of Ncd and Ase1.

Previously, it has not been clear how motorized microtubule sliding, important for self-organization of microtubule networks, can locally be slowed down to maintain stable overlaps between antiparallel microtubules. Sets of opposing motors were proposed to regulate sliding velocity but this mechanism seems vulnerable to natural variations in motor stoichiometry[5,6]. On the basis of the action of passive crosslinkers, we describe a braking mechanism that adapts itself to local microtubule geometry: microtubules that steadily slide along other microtubules slow down only when the microtubules start to slide apart. For this to work, two requirements have to be met: crosslinkers have to be retained within the shrinking microtubule overlap and slowdown needs to be dose dependent. A feedback loop makes the mechanism inherently robust; motor-propelled separation of microtubules progressively compacts the crosslinkers and slows down further sliding. Consequently, full separation of microtubules is prevented over a wide range of parameter values (Supplementary Fig. S5c). Reported interactions between Ase1 homologues and motors will generate an additional layer of feedback that needs to be addressed in future work[16,21].

To stall microtubule sliding, we found that about four times more Ase1 linkers than Ncd motors must bind in overlaps. For PRC1 crosslinkers in combination with Eg5 motors, a ratio of 25:1 slowed down sliding by a factor of 2 (ref. 22). Apart from differences between Ase1 and PRC1, the higher ratio may also originate from the fact that Ncd, being a non-processive motor with a tail domain that diffuses on microtubules, is a weaker force generator than Eg5 operating with active motor domains on both microtubules[3,5]. Nonetheless, both works show that passive crosslinkers slow down motorized sliding.

The physical mechanism underlying microtubule slowdown is presumably related to friction generated between crosslinkers and moving microtubules[23]. However, we did not find the sliding velocity to decrease asymptotically with density (Fig. 4a), as in a model in which a linear force–velocity relation for motors was assumed and multiple passive crosslinkers were treated as independent viscous friction generators that add up linearly[5]. Instead, the sliding velocity decreased linearly with density up to a stopping density, indicating that the previous assumptions do not hold for the Ase1–Ncd pair. We expect that cells maintain equilibrium linker/motor ratios below the stopping threshold to allow for network formation through microtubule sliding[24,25].

Compaction of Ase1 in shortening overlaps is driven by molecular sweeping at microtubule ends. It is remarkable that Ase1 combines all three properties that are required for sweeping: lattice diffusion; a difference in affinity between single microtubules and microtubule overlaps—on average the Ase1–GFP signal is 12.0 ± 1.3-fold (±s.e.m.; $n = 9$) increased in microtubule overlaps relative to single microtubules (Fig. 1c); and a low molecular off-rate to make compaction persistent. Adaptive braking is enabled because Ncd has no increased affinity for overlaps and hence does not accumulate by sweeping—the GFP–Ncd signal is only 2.3 ± 0.2-fold (±s.e.m.; $n = 19$) increased in overlaps relative to single microtubules (Figs 1d and 2d). *In vivo* evidence indicates that the molecular properties of Ase1 are in the correct range to enable adaptive braking. First, reported off-rates for yeast and several plant homologues of Ase1 in anaphase are similar to our measured value for Ase1–GFP *in vitro*[11,13,26]. Second, we observed sweeping in overlaps due to depolymerization of microtubule plus-ends in *S. pombe* cells (Supplementary Fig. S6 and Movie S5). Fast turnover of the human homologue of Ase1, PRC1, on the other hand, explains why sweeping and accumulation has not been previously observed *in vitro*[29]. However, turnover of Ase1 and oligomerization of PRC1 are phosphoregulated, indicating that accumulation in cells may depend on the phosphorylation state[15,16,27]. It is worth noting that sweeping is a physical phenomenon related to microtubule ends acting as diffusion barriers. It may thus be more generally exploited by other filamentous systems and crosslinking proteins.

Sweeping occurs independently of the motor used, as demonstrated here by *Drosophila* Ncd and *S. pombe* Klp2. It may thus similarly occur when the sliding direction is reversed. In the spindle midzone, overlapping microtubule plus-ends are driven apart by plus-end-directed motors such as Eg5 and Mklp1. Although we did not study sweeping for a plus-end-directed motor that functions simultaneously

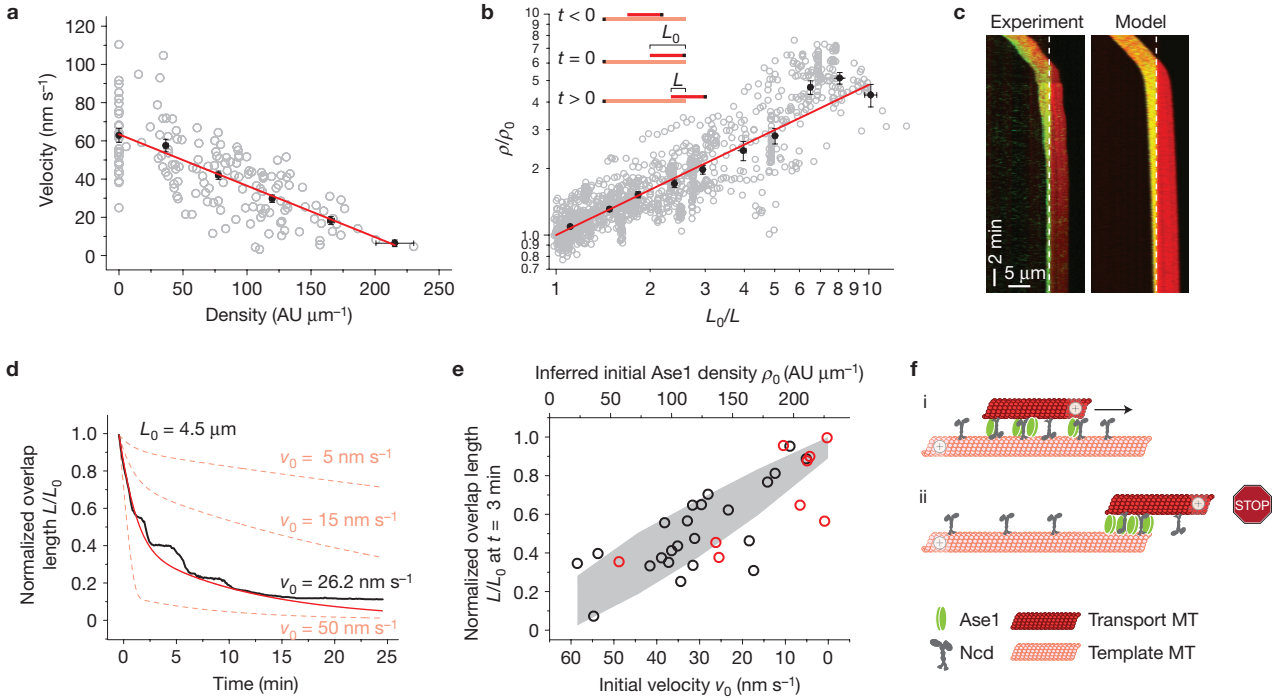

Figure 4 Quantitative description of microtubule overlap dynamics. (**a**) Instantaneous microtubule sliding velocity as function of Ase1–GFP density for 127 transport microtubules (including 27 measurements in the absence of Ase1–GFP). Within each bin, values that belong to the same microtubule were first averaged (grey circles; bin width is 50 AU µm^{-1}). Black dots denote averaged values of the grey data in each bin (±s.e.m.). The red line shows a linear fit to the average velocities within the bins (see Methods). (**b**) Normalized Ase1–GFP density ρ/ρ_0 versus L_0/L, the inverse of the normalized overlap length. Grey circles represent time points from 51 events of transport microtubule stalling at template ends. Black dots are binned averages (±s.e.m.) of the grey data. The red line shows a linear fit of equation (2) in the Methods to the black data. Densities are derived from measured velocities using the linear relationship established in **a** (see Methods). (**c**) Multi-colour kymographs showing the formation of stable microtubule overlaps between template microtubule (dim red) and transport microtubule (bright red) in the presence of Ase1–GFP (green). Experimental data (left) and model constructed from artificially generated microscope images (right). (**d**) Normalized overlap lengths L/L_0 for the event in **c** (experimental data in black and model calculations in red). The measured sliding velocity v_0 and the length of the transport microtubule, L_0, are indicated. The dashed pale red curves indicate model calculations for different values of v_0. (**e**) Normalized overlap length L/L_0 at t_0+3 min versus Ase1–GFP density ρ_0 for all events where overlap shrinkage lasted at least 4 min ($n=32$). The grey area indicates model outcomes for a corresponding range of L_0 and k_{on} (Methods). Red points indicate the steady-state events shown in Supplementary Fig. S5b. (**f**) Schematic representation of the motorized formation of stable antiparallel microtubule overlaps in the presence of Ase1. i, Ncd in the overlap slides microtubules in the presence of Ase1 at low density. ii, During microtubule separation, Ase1 becomes compacted through molecular sweeping, whereas the density of Ncd does not change. As a result microtubule sliding progressively slows down.

with Ase1 during mitosis, our results indicate that crosslinkers of the Ase1/PRC1 family may become enriched through sweeping in microtubule overlaps of spindles. The concurrent slowdown of sliding would prevent the separation of microtubules and may explain in part why spindles break prematurely in the absence of Ase1 homologues[11–14]. Such a physical mechanism could act in synergy with biochemical control of microtubule dynamics to ensure the integrity and organization of spindles. Recently it was shown that CLASP and Xklp1 are recruited by Ase1 homologues to prevent the disassembly of overlapping microtubules[28,29]. How microtubule sliding by motors will affect these regulatory processes is not clear. It will be interesting to combine Ase1 regulation of plus-end-directed motors with control over microtubule dynamics to study the sliding between dynamic microtubule plus-ends *in vitro*. □

METHODS

Methods and any associated references are available in the online version of the paper at http://www.nature.com/naturecellbiology

Note: Supplementary Information is available on the Nature Cell Biology website

ACKNOWLEDGEMENTS

We thank C. Bräuer for technical assistance; J. Teapal and T. Toda for yeast strains; and R. Schneider, M. Zanic, M. Gardner, J. Howard and B. Mulder for discussions. M.B. and S.D. acknowledge support from the European Research Council (ERC starting grant); G.F. from Boehringer Ingelheim Fonds; S.D. from the Deutsche Forschungsgemeinschaft (DFG Heisenberg Programme); and M.E.J. from the Division for Earth and Life Sciences (ALW) with financial aid from the Netherlands Organization for Scientific Research (NWO).

AUTHOR CONTRIBUTIONS

M.B., Z.L., G.F., S.D. and M.E.J. designed the experiments; M.B., Z.L. and G.F. carried out the experiments; M.B., Z.L., G.F. and F.R. analysed the data; Z.L. and M.E.J. developed the model; M.B., Z.L., M.E.J. and S.D. wrote the manuscript; M.E.J. and S.D. initiated the research and supervised the work. All authors discussed the results and commented on the manuscript.

COMPETING FINANCIAL INTERESTS

The authors declare no competing financial interests.

Published online at http://www.nature.com/naturecellbiology
Reprints and permissions information is available online at http://www.nature.com/reprints

1. Goshima, G. & Scholey, J. M. Control of mitotic spindle length. *Annu. Rev. Cell Dev. Biol.* **26,** 21–57 (2010).

2. Braun, M., Drummond, D. R., Cross, R. A. & McAinsh, A. D. The kinesin-14 Klp2 organizes microtubules into parallel bundles by an ATP-dependent sorting mechanism. *Nat. Cell Biol.* **11,** 724–730 (2009).
3. Fink, G. *et al.* The mitotic kinesin-14 Ncd drives directional microtubule–microtubule sliding. *Nat. Cell Biol.* **11,** 717–723 (2009).
4. Kapitein, L. C. *et al.* The bipolar mitotic kinesin Eg5 moves on both microtubules that it crosslinks. *Nature* **435,** 114–118 (2005).
5. Hentrich, C. & Surrey, T. Microtubule organization by the antagonistic mitotic motors kinesin-5 and kinesin-14. *J. Cell Biol.* **189,** 465–480 (2010).
6. Tao, L. *et al.* A homotetrameric kinesin-5, KLP61F, bundles microtubules and antagonizes Ncd in motility assays. *Curr. Biol.* **16,** 2293–2302 (2006).
7. Vale, R. D., Malik, F. & Brown, D. Directional instability of microtubule transport in the presence of kinesin and dynein, two opposite polarity motor proteins. *J. Cell Biol.* **119,** 1589–1596 (1992).
8. Manning, A. L. & Compton, D. A. Structural and regulatory roles of nonmotor spindle proteins. *Curr. Opin. Cell Biol.* **20,** 101–106 (2008).
9. Janson, M. E. *et al.* Crosslinkers and motors organize dynamic microtubules to form stable bipolar arrays in fission yeast. *Cell* **128,** 357–368 (2007).
10. Peterman, E. J. G. & Scholey, J. M. Mitotic microtubule crosslinkers: insights from mechanistic studies. *Curr. Biol.* **19,** R1089–R1094 (2009).
11. Loiodice, I. *et al.* Ase1p organizes antiparallel microtubule arrays during interphase and mitosis in fission yeast. *Mol. Biol. Cell* **16,** 1756–1768 (2005).
12. Mollinari, C. *et al.* PRC1 is a microtubule binding and bundling protein essential to maintain the mitotic spindle midzone. *J. Cell Biol.* **157,** 1175–1186 (2002).
13. Schuyler, S., Liu, J. & Pellman, D. The molecular function of Ase1p: evidence for a MAP-dependent midzone-specific spindle matrix. Microtubule-associated proteins. *J. Cell Biol.* **160,** 517–528 (2003).
14. Yamashita, A., Sato, M., Fujita, A., Yamamoto, M. & Toda, T. The roles of fission yeast ase1 in mitotic cell division, meiotic nuclear oscillation, and cytokinesis checkpoint signaling. *Mol. Biol. Cell* **16,** 1378–1395 (2005).
15. Khmelinskii, A., Roostalu, J., Roque, H., Antony, C. & Schiebel, E. Phosphorylation-dependent protein interactions at the spindle midzone mediate cell cycle regulation of spindle elongation. *Dev. Cell* **17,** 244–256 (2009).
16. Fu, C. *et al.* Phospho-regulated interaction between kinesin-6 Klp9p and microtubule bundler Ase1p promotes spindle elongation. *Dev. Cell* **17,** 257–267 (2009).
17. Kapitein, L. C. *et al.* Microtubule-driven multimerization recruits ase1p onto overlapping microtubules. *Curr. Biol.* **18,** 1713–1717 (2008).
18. Gestaut, D. R. *et al.* Phosphoregulation and depolymerization-driven movement of the Dam1 complex do not require ring formation. *Nat. Cell Biol.* **10,** 407–414 (2008).
19. Powers, A. F. *et al.* The Ndc80 kinetochore complex forms load-bearing attachments to dynamic microtubule tips via biased diffusion. *Cell* **136,** 865–875 (2009).
20. Gardner, M. K. & Odde, D. J. Dam1 complexes go it alone on disassembling microtubules. *Nat. Cell Biol.* **10,** 379–381 (2008).
21. Gruneberg, U. *et al.* KIF14 and citron kinase act together to promote efficient cytokinesis. *J. Cell Biol.* **172,** 363–372 (2006).
22. Subramanian, R. *et al.* Insights into antiparallel microtubule crosslinking by PRC1, a conserved nonmotor microtubule binding protein. *Cell* **142,** 433–443 (2010).
23. Bormuth, V., Varga, V., Howard, J. & Schäffer, E. Protein friction limits diffusive and directed movements of kinesin motors on microtubules. *Science* **325,** 870–873 (2009).
24. Burbank, K. S., Mitchison, T. J. & Fisher, D. S. Slide-and-cluster models for spindle assembly. *Curr. Biol.* **17,** 1373–1383 (2007).
25. Loughlin, R., Heald, R. & Nédélec, F. A computational model predicts *Xenopus* meiotic spindle organization. *J. Cell Biol.* **191,** 1239–1249 (2010).
26. Smertenko, A. P. *et al.* The C-terminal variable region specifies the dynamic properties of *Arabidopsis* microtubule-associated protein MAP65 isotypes. *Plant Cell* **20,** 3346–3358 (2008).
27. Zhu, C., Lau, E., Schwarzenbacher, R., Bossy-Wetzel, E. & Jiang, W. Spatiotemporal control of spindle midzone formation by PRC1 in human cells. *Proc. Natl Acad. Sci. USA* **103,** 6196–6201 (2006).
28. Bratman, S. V. & Chang, F. Stabilization of overlapping microtubules by fission yeast CLASP. *Dev. Cell* **13,** 812–827 (2007).
29. Bieling, P., Telley, I. A. & Surrey, T. A minimal midzone protein module controls formation and length of antiparallel microtubule overlaps. *Cell* **142,** 420–432 (2010).

METHODS

Protein purification. Recombinant histidine-tagged full-length *S. pombe* Ase1, Ase1–GFP and Klp2 and *Drosophila melanogaster* Ncd and GFP–Ncd were expressed and purified as described previously[2,3,9].

***In vitro* motility assay.** Microtubules and flow chambers were prepared as described previously[3]. First, biotinylated template microtubules, dimly labelled with rhodamine, were immobilized in a flow chamber using biotin antibodies (Sigma B3640, 40 μg ml^{-1} in PBS; ref. 3). In the second step, Ncd and Ase1 were flushed into the flow cell at final assay concentrations. In the third step, brightly labelled, non-biotinylated transport microtubules were flushed into the flow cell and bound to the template microtubules that were still covered sparsely with Ase1 and Ncd from the second step. In the final fourth step, the chamber was rinsed with assay buffer containing Ncd and Ase1 at assay concentrations. This last step removed unbound transport microtubules from solution. Assays were carried out at physiological ionic strength in assay buffer (20 mM HEPES at pH 7.2, 1 mM EGTA, 0.1 mM EDTA, 75 mM KCl, 1 mM ATP (+Mg), 10 mM dithiothreitol, 0.5 mg ml^{-1} casein, 10 μM paclitaxel, 0.1% Tween, 10% w/v sucrose, 20 mM D-glucose, 110 μg ml^{-1} glucose oxidase and 20 μg ml^{-1} catalase). To visualize diffusion of transport microtubules, the fourth step in the sample preparation was omitted and only Ase1–GFP was added in the second step at 0.78 nM, which was then diluted out in the third step (Fig. 2a). To visualize diffusion of single Ase1–GFP molecules between sliding microtubules, the fourth step was omitted and Ase1–GFP and Ncd were added in the second step at 0.78 nM and 1.16 nM concentrations, respectively.

Imaging. Rhodamine-labelled microtubules and GFP-labelled proteins (either Ncd or Ase1) in microtubule sliding assays were visualized sequentially by switching between GFP and TRITC (tetramethyl rhodamine *iso*thiocyanate) filters (Chroma Technology) using a previously described set-up[3] at an acquisition rate of 1 frame per 6 seconds. FRAP (fluorescence recovery after photobleaching) experiments with GFP-labelled Ase1 were carried out using a Nikon Eclipse Ti microscope (×100/1.4 NA oil-immersion objective) equipped with a Roper Scientific SAS FRAP unit. Fluorescence recovery was visualized using an attached spinning-disc confocal unit (CSU-X1, Yokogawa) in combination with a QuantEM EMCCD camera (Photometrics). The post-FRAP acquisition rate was 2 frames per minute. FRAP experiments on Ase1–GFP were carried out in the absence of motors using the same sample chamber preparation and buffer conditions as in the motility assays.

Image analysis. Using FIESTA tracking software[30] we obtained the positions of transport microtubules in each frame of the acquired movies. Tracking was stopped if the transport microtubule interacted with a second template microtubule or another transport microtubule. The frame at which the transport microtubule reached the end of the template microtubule, t_0, was selected manually. The length of a shrinking overlap was calculated from the displacement of the leading end of the transport microtubule relative to its position at t_0. The position of the overlap determined from the rhodamine channel was used as a mask to read out the total amount of overlap-bound Ase1–GFP (in arbitrary units—AU). The Ase1–GFP signal in a region directly adjacent to the mask was subtracted as the background signal.

Velocity–density analysis. Sliding velocities were obtained from positional data of the transport microtubules using a rolling frame average over 9 frames. Ase1–GFP densities were determined by the GFP fluorescence intensities in the microtubule overlap regions defined by the positions of the transport microtubules. We prevented a severe underestimation of the Ase1–GFP densities due to photobleaching by analysing only data taken during the first 2 min (corresponding to 20 single-frame exposures) after the final addition of Ase1–GFP and Ncd. The residual impact of photobleaching is estimated to be between 0 and −23% (time constant of photobleaching 420 ± 24 s; ±s.e.m., 8 movies analysed, obtained by imaging sparse amounts of surface-absorbed Ase1–GFP under identical illuminating conditions as used in our sliding assays).

Data were acquired in a total of 27 flow chambers on 5 different days. Figure 4a contains results from 127 sliding microtubules (100 microtubules in the presence of Ncd and Ase1–GFP; 27 microtubules in the presence of Ncd alone). All time points were binned in 5 bins ranging from $\rho = 0$ AU μm^{-1} to $\rho = 250$ AU μm^{-1} with steps of $\Delta\rho = 50$ AU μm^{-1}. A sixth bin was added that contained the measurements acquired in the absence of Ase1 ($\rho = 0$ AU μm^{-1}). Time points within a bin that belonged to a single microtubule were first averaged. Next, these values were averaged for all microtubules that contributed to a certain bin. In this way, all microtubules within a bin were weighted equally.

Modelling overlap dynamics. The starting point of the model calculations is t_0 at which a transport microtubule of length L_0 has reached the end of the template microtubule with a velocity v_0 (subscript 0 indicates a value at t_0). We model Ase1 compaction and turnover to predict the subsequent time evolution of the overlap length. If sweeping would be 100% efficient, all Ase1 would be retained in the overlap and the Ase1 density, ρ, would double each time the overlap length is halved. Generally, we expect the relative increase in density to be proportional to the relative decrease in overlap length L. The proportionality factor is the compaction efficiency ε:

$$\frac{\mathrm{d}\rho}{\rho} = -\varepsilon\frac{\mathrm{d}L}{L} \tag{1}$$

This equation can be solved as:

$$\ln\left(\frac{\rho}{\rho_0}\right) = \varepsilon\ln\left(\frac{L_0}{L}\right) \tag{2}$$

In principle, this equation can be used to infer efficiency from observed density changes during overlap shortening (Fig. 2b). Molecular turnover, not included in the equation, does however contribute to density changes experimentally. To limit this contribution, we selected data to minimize for two effects. First, the initial build-up of Ase1 after its addition to the sample (Fig. 1e) can still be ongoing at the time the transport microtubule reaches the template end. The average timescale of this initial rise was 186 ± 30 s (±s.e.m.; single exponential fit to the average curve of 16 events) and equals the sum of the on- and off- rates[31]. To exclude this build-up phase from our data, we exclusively analysed those microtubules that had been sliding for 6 min or longer before reaching the template end ($n = 9$) and assumed that they had reached steady-state conditions. Second, any accumulation of Ase1 through sweeping above equilibrium levels will decay with the molecular off-rate (Supplementary Fig. S5a, about 10 min). We therefore limited the data to densities measured during the first 3 min after the initiation of microtubule separation. Fitting equation (2) to data that obey both constraints yielded a sweeping efficiency of 0.62 ± 0.03 for a limited set of 9 microtubules. After we released the first constraint and included microtubules that may not have yet reached equilibrium at t_0, we still found an excellent fit to the data and a slightly higher efficiency of 0.72 ± 0.06 (±s.e.m.; Fig. 4b; correlation coefficient of fitted data is 0.88, $P = 0$). We continued using the latter efficiency for our calculations because it is based on a more substantial set of 54 microtubules. The final choice between the two efficiency values did not significantly change the outcome of our model as described below.

To calculate the change in the Ase1 distribution within the overlap due to sweeping and turnover we use $n = L\rho$ and $\mathrm{d}n = L\mathrm{d}\rho + \rho\mathrm{d}L$. Retainment of Ase1 can be calculated by substitution of equation (1):

$$\mathrm{d}n_{\mathrm{sweeping}} = n(1-\varepsilon)\frac{\mathrm{d}L}{L} \tag{3}$$

The total change of Ase1 in the overlap includes sweeping and turnover at rates k_{on} and k_{off}:

$$\frac{\mathrm{d}n}{\mathrm{d}t} = \frac{n}{L}(1-\varepsilon)\frac{\mathrm{d}L}{\mathrm{d}t} + k_{\mathrm{on}}L - k_{\mathrm{off}}n \tag{4}$$

In addition, the change in overlap length is given by:

$$\frac{\mathrm{d}L}{\mathrm{d}t} = -v(\rho) \tag{5}$$

with $v(\rho)$ being the linear relationship between density and velocity as fitted in Fig. 4a ($v = -0.28\rho + 64$; correlation coefficient of the fitted data is -0.7, $P = 10^{-25}$).

Changes in L and n (Equations (4) and (5)) were calculated and integrated numerically from t_0 to t using an Euler forward integration scheme. Calculations for a particular microtubule required values for k_{on}, n_0 and L_0 in addition to the known values of k_{off} and ε. L_0 was obtained from the tracking algorithm, but the number of Ase1–GFP molecules at t_0 (n_0) could not be obtained reliably from intensity measurements because of photobleaching. Instead we calculated n_0 using the $v(\rho)$ relationship knowing v_0 and L_0. The actual on-rate varied from sample to sample owing to changes in Ase1 and microtubule concentrations. Therefore, we estimated k_{on} from steady-state Ase1–GFP levels in the overlap after the initial build-up phase was over. Again, we used the 9 transport microtubules (out of 54 analysed terminal overlaps) that were sliding for more than 6 min before reaching the end of the template microtubule. For these events, v_0 gave us ρ_0, which was then used as the steady-state Ase1–GFP level ρ_{SS}. At t_0, the sweeping term in equation (4) is still zero and we can rewrite the equation in the steady state as $k_{\mathrm{on}} = \rho_{\mathrm{SS}}k_{\mathrm{off}}$. For the 9 events, the model was calculated as shown in Fig. 4c,d and Supplementary Fig. S5b.

In Fig. 4e the relative length of the overlap at 3 min after t_0 was plotted versus ρ_0 (note that ρ_0 is now not necessarily equal to ρ_{SS} and $n = 32$ because not all

DOI: 10.1038/ncb2323

terminal overlaps were observed for 3 min or longer). To determine whether the observed trend is in agreement with our model we calculated the model for the experimentally relevant range of L_0 (0.5–11.0 μm, corresponding to the length of the 32 microtubules) and k_{on} (0.28–0.38 AU $\mu m^{-1}s^{-1}$ corresponding to 0.03–0.04 Ase1 dimers $\mu m^{-1}s^{-1}$). This range of k_{on} was obtained from measurements on 27 microtubules within the given length range that were sliding for more than 6 min along the template microtubule without reaching the end. The outcome of the model calculations is depicted as the grey area in Fig. 4e and shows that most events are contained within the model.

30. Ruhnow, F., Zwicker, D. & Diez, S. Tracking single particles and elongated filaments with nanometer precision. *Biophys. J.* **100,** 2820–2828 (2011).
31. Pollard, T. D. A guide to simple and informative binding assays. *Mol. Biol. Cell* **21,** 4061–4067 (2010).

nature cell biology

DOI: 10.1038/ncb2323

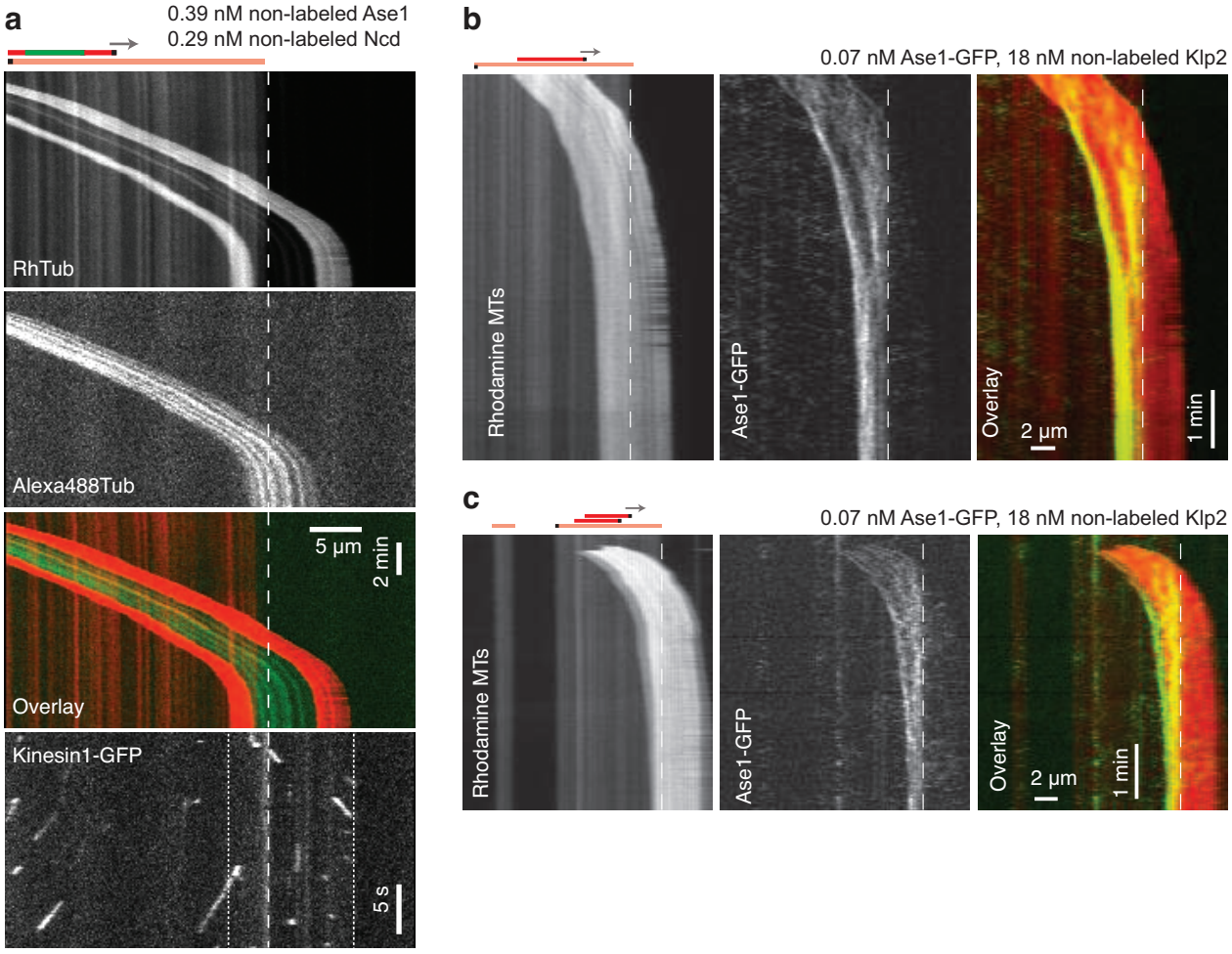

Figure S1 Analysis of transport MT slowdown at the end of template MTs. **(a)** Multi-channel kymographs of an experiment similar to Fig. 2a using non-labeled Ase1 and non-labeled Ncd (upper three panels). MT polarities are schematically depicted above the top kymograph. Alexa488-labeled transport MT seeds are extended by rhodamine-labeled MT ends. The longer rhodamine-labeled end of the transport MT is the MT plus end. The polarity of the template MT was determined by addition of GFP-labeled kinesin-1 molecules, which moved towards MT plus-ends (bottom kymograph). GFP-labeled kinesin-1 molecules on the transport MT moved in opposite direction to those on the template MT and are both MTs are thus arranged in an antiparallel fashion. **(b)** To verify that the observed slowdown of transport MTs in Fig. 2 is not specific to the use of *Drosophila* kinesin-14 Ncd motors, we initiated sliding with Klp2 motors from *S. pombe*. After addition of Ase1-GFP, we observed a slowdown of MT sliding and an accumulation of Ase1-GFP in the overlap region when the transport MT starts to slide apart from the template MT. Persistent overlaps were formed. Two typical multi-channel kymographs are shown. Dashed lines indicate the position of the template MT minus-end. These results indicate that adaptive braking occurs independent of the motor species that drives MT sliding.

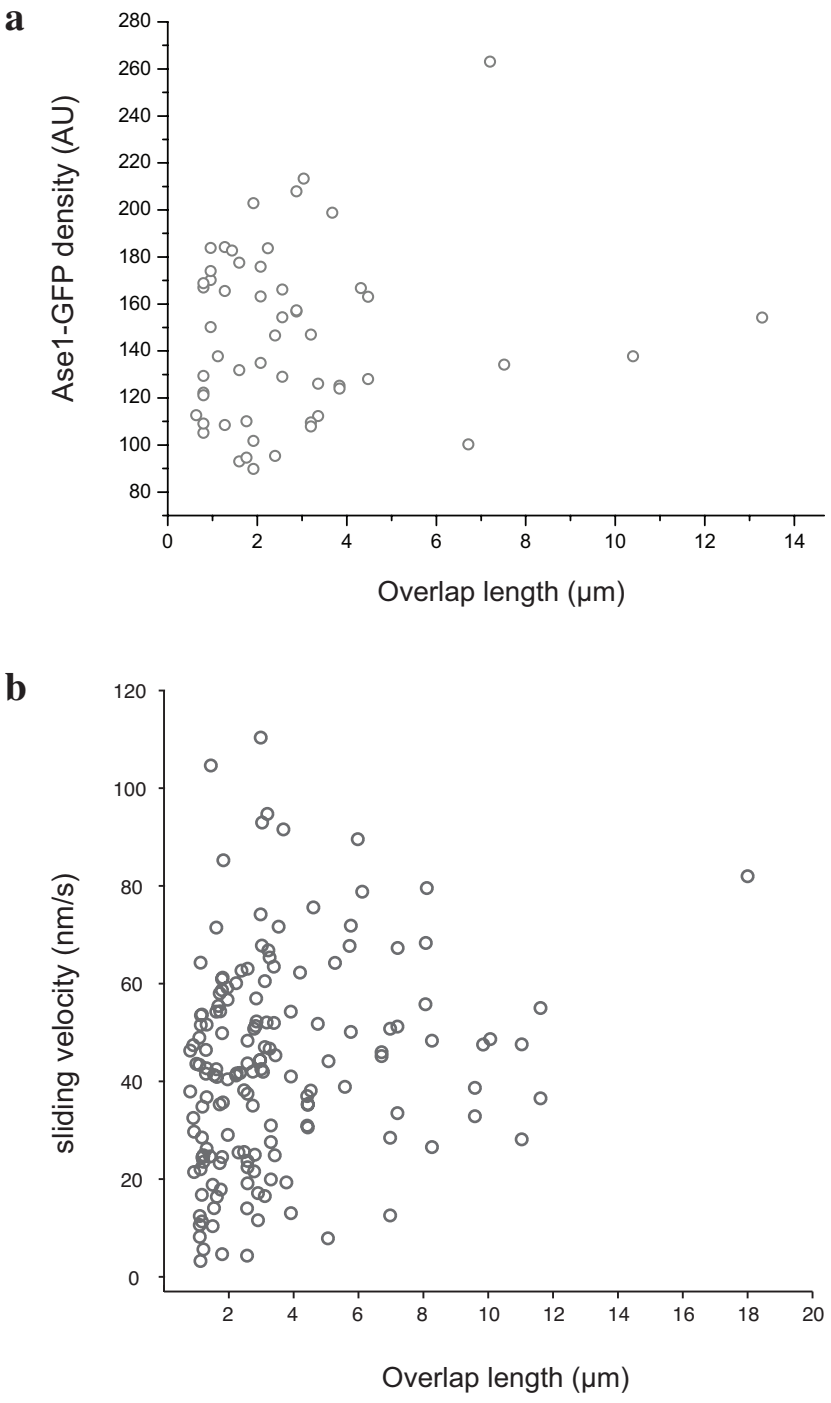

Figure S2 Sliding velocity and Ase1 density do not depend on MT length. **(a)** Ase1-GFP density in MT overlaps in the absence of motors as a function of the overlap length. 54 overlaps were analysed yielding a correlation coefficient of 0.1 with a 95% confidence interval from -0.17 to 0.36 and a p-value of 0.46. **(b)** MT sliding velocity as function of MT length for 127 transport MTs (including 27 measurements in absence of Ase1-GFP). The correlation coefficient for this data is 0.2130 with a 95% confidence interval from 0.0583 to 0.3577 and a p-value of 0.0074.

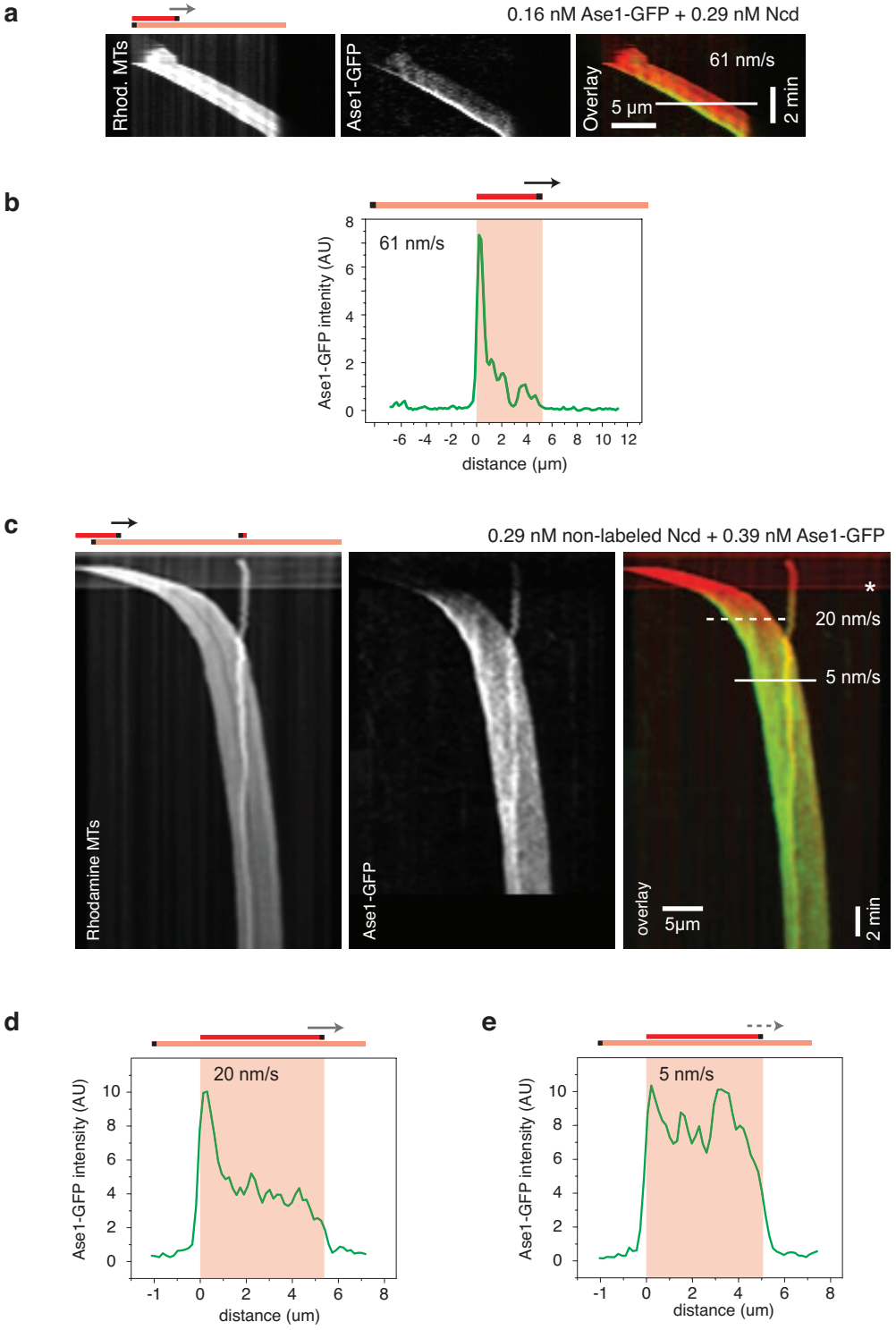

Figure S3 Sweeping of Ase1-GFP is pronounced at fast moving transport MTs. **(a)** Multi-channel kymographs of an experiment similar to Fig. 1c using Ncd and low concentration of Ase1-GFP (MT polarities are schematically depicted above the kymograph). **(b)** The intensity profile along the white line in (a) clearly shows strong accumulation of Ase1-GFP at the trailing end of this fast moving transport MT (average velocity is 61 nm/s). **(c)** Multi-channel kymographs as in Fig. 1c but constructed for an extended time. **(d)** Intensity profile along the dashed white line in (c) 2 min after flush-in of Ase1 (sliding velocity is 20 nm/s). Ase1-GFP end accumulation is not as strong as for the faster sliding MT shown in a and b (**e**) Intensity profile along the solid white line in (c) 6 min after flush-in of Ase1-GFP (sliding velocity is 5 nm/s). Ase1-GFP end accumulation was not detectable.

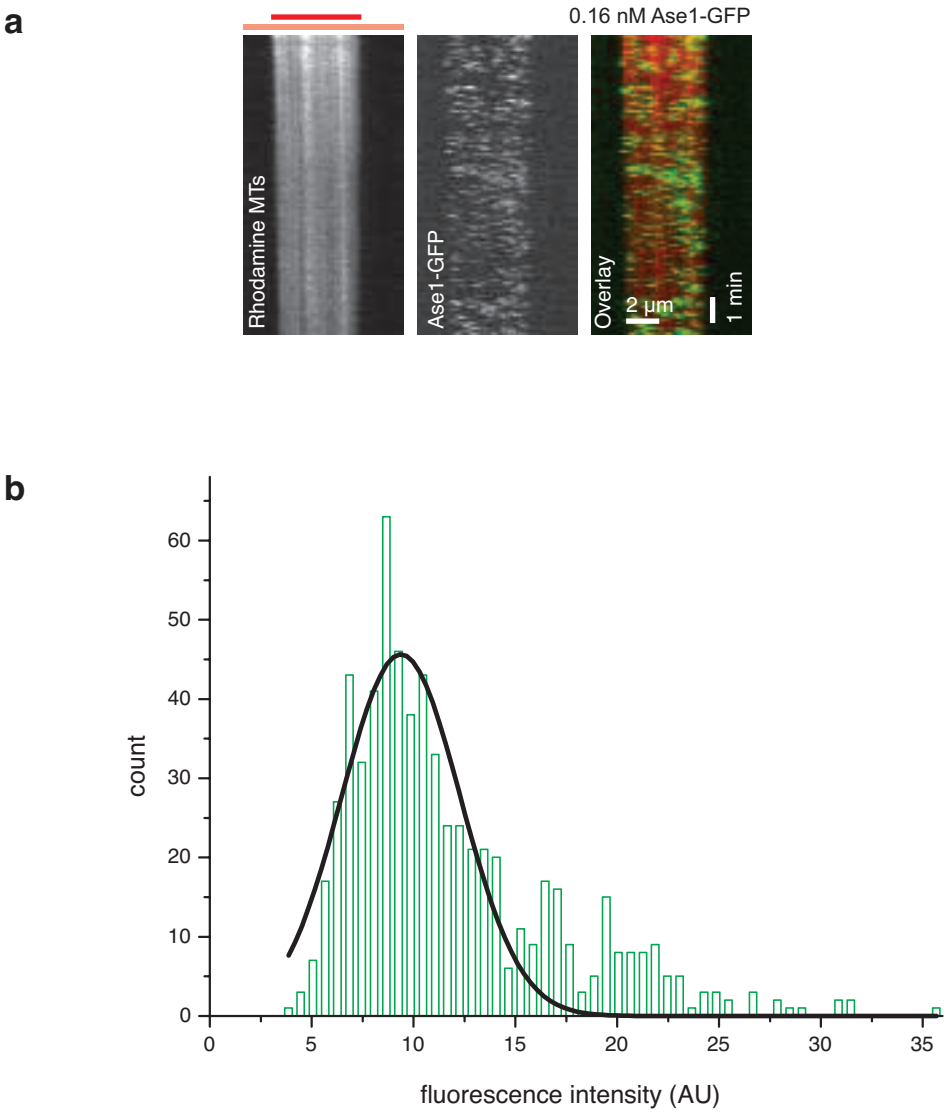

Figure S4 Quantification of single molecule Ase1-GFP fluorescence intensity. **(a)** Multi-channel kymograph of individual Ase1-GFP spots on single MTs (Movie S3). **(b)** Earlier work identified such spots as Ase1 dimers[17]. 569 individual spots were selected by hand and the 2D intensity profile was fitted with a 5-parameter 2D Gaussian fit (XY center position, intensity offset, peak intensity, and width). Offset-subtracted pixel intensities around the center position were integrated over 1.6 µm x 1.6 µm areas. The histogram in (b) shows a major peak centered around 9.4 AU. The tail of the histogram may have been caused by the temporary presence of multiple dimers within a single diffraction-limited spot. The dimer intensity (9.4 AU) provides the conversion factor for the measured intensities in AU in the main text.

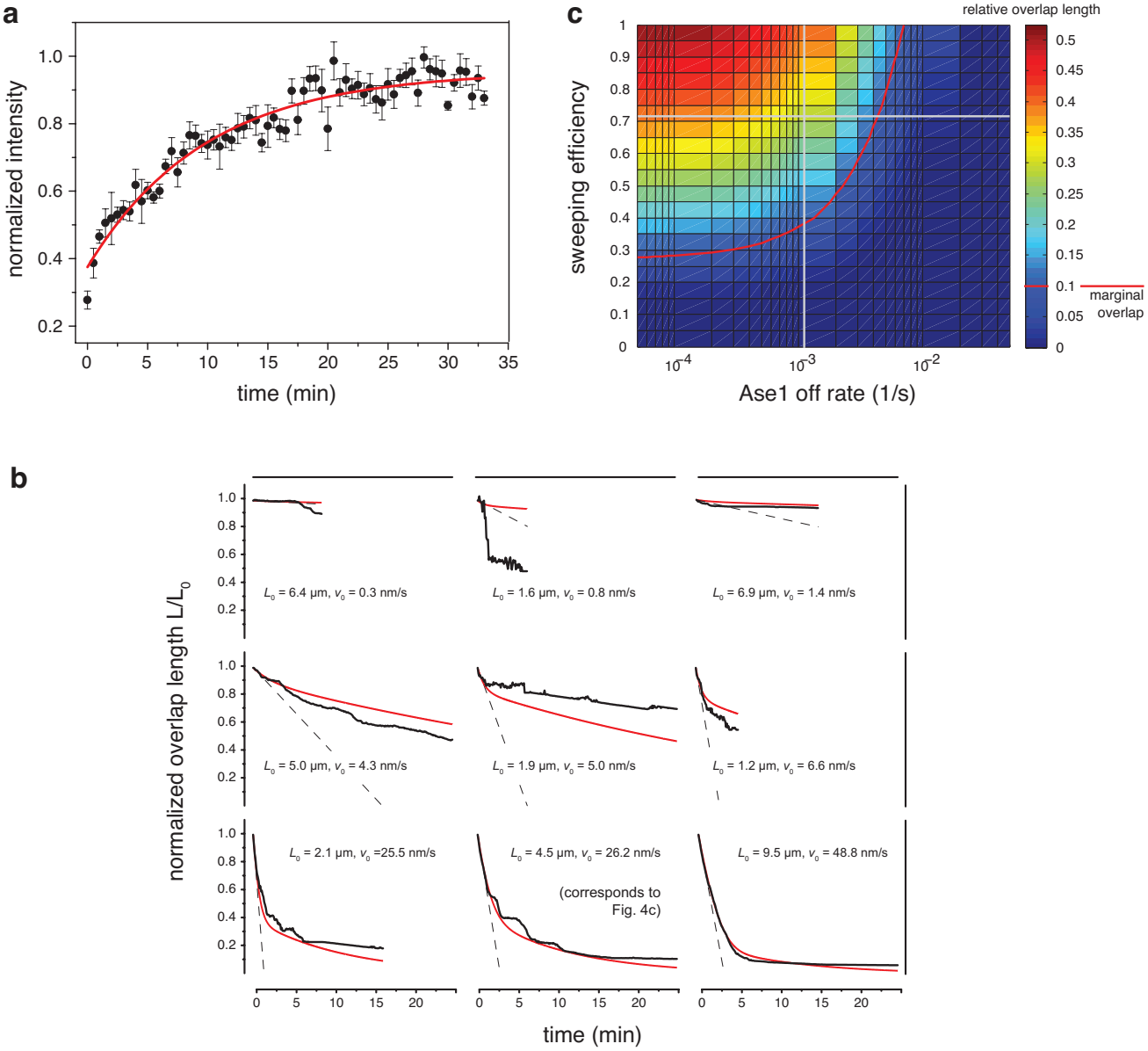

Figure S5 Model parameters and model results **(a)** FRAP of Ase1-GFP fluorescence averaged for 13 MTs in the absence of Ncd motors (±SE). Pre-FRAP intensity was normalized to 1. Exponential fit $I_N = 1 - ae^{-\tau/t}$; $\tau_{recovery}$ = 590 ± 57 s; $k_{off} = 1/\tau_{recovery}$. **(b)** Data as in Fig. 4d for all events where sliding proceeded for longer than 6 min before the start of overlap shrinkage. The dashed lines indicate the predicted dynamics if sliding would not have been slowed down by Ase1 compaction. **(c)** Sensitivity of model to variations in the key model parameters: (i) the sweeping efficiency varied between 0 and 1 and (ii) the Ase1 off-rate varied between 1/20000 s^{-1} and 1/20 s^{-1} (grey lines - measured values ε = 0.72 and k_{off} = 1/590 s^{-1}). The molecular on-rate was changed along with the off-rate (k_{on}/k_{off} = constant) in order to keep the steady state density constant. Results were calculated for a transport MT with a typical length of 4 µm which had reached a steady state Ase1-GFP density of 114 AU/µm when it started to slide apart from the template MT. At this density the sliding velocity equals 50% of the maximum sliding velocity for Ncd (34 nm/s, see Fig. 4a). If sliding would have continued at the same pace both MTs would be fully separated after 2.2 minutes. The modeled relative overlap length after 10 minutes of sliding is plotted in a color-coded manner. Red line demarcates the area with significant relative overlaps of 0.1 or more (absolute overlap 0.4 µm). This simple analysis demonstrates that adaptive braking would still be effective at parameter values that are less optimal than Ase1 values (lower sweeping efficiencies or faster rates of turnover).

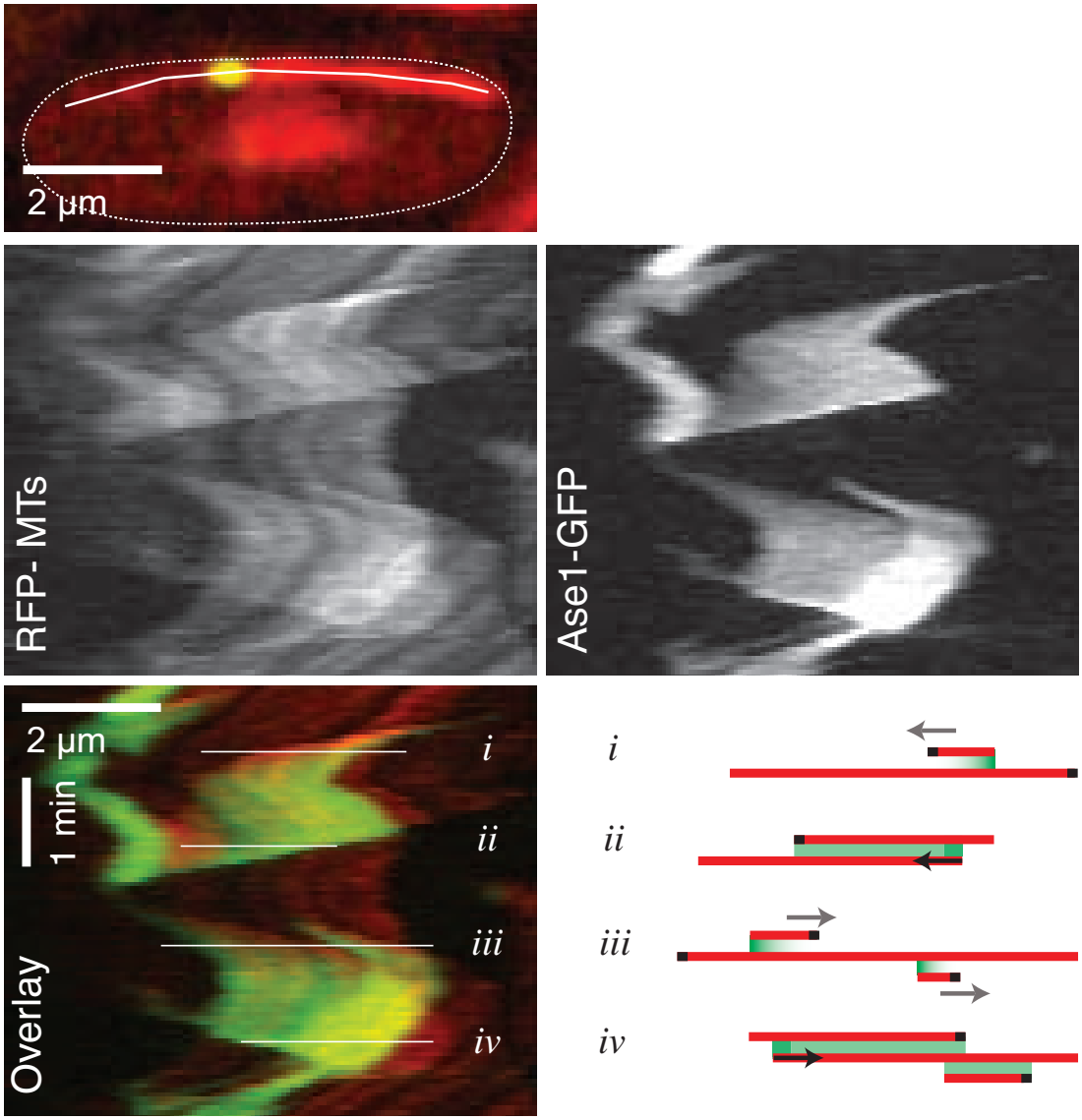

Figure S6 Ase1 distribution at moving MT ends *in vivo.* Multi-channel kymographs illustrating the dynamics of an interphase MT bundle (mRFP-tubulin and Ase1-GFP) in *S. pombe* (movie S5; first frame is shown). Schematic shows inferred MT polarities (ref. 9 and Janson, M.E. et al. 2005 *J Cell Biol* **169**, 297-308) along the white lines for four different time points (black dots mark plus ends, black arrows mark depolymerizing plus ends). New MTs are added to bundles by anti-parallel nucleation along existing MTs and older MTs are removed by catastrophes. Sliding of new MTs is powered by Klp2 and slows down as MTs elongate. At time point i, a newly nucleated MT grew along a long MT growing to the right. At ii, the underlying MT had a catastrophe and depolymerized along the new MT. At iii, two new MTs were nucleated along a MT that grew to the left and which had a catastrophe at time point iv. Green gradients in the schematic indicate observed differences in Ase1-GFP levels near moving MT ends. Ase1-GFP signals along sliding nascent MTs were often enhanced at the trailing minus-ends compared to the growing plus-ends (i and iii) suggesting that sweeping occurs. However, given an off-rate for Ase1 in interphase cells of 1 / (17.0 ± 1.5 s^{-1}) (ref. 9) and an initial MT growth velocity in the analyzed cells of 30 ± 5 nm/s (n=18), the terminal ~0.5 µm near a growing plus-end are expected to have a low amount of associated Ase1-GFP providing an alternative explanation for the gradient. We hypothesized that depolymerizing plus-ends within MT bundles (ii and iv) should also form a moving barrier for Ase1 diffusion. A significant accumulation of Ase1-GFP was observed at the shrinking side of the MT overlaps, a strong indication that sweeping does occur *in vivo.* Ase1-GFP was thus retained in the shortening overlap analogous to the accumulation observed on sliding ends *in vitro.* Accumulation is best observed in the mono color kymograph for Ase1-GFP. *Methods associated to this figure: S. pombe* cells expressing mRFP-atb2 (beta-tubulin; Sato, M. et al. 2009 *Methods Mol Biol* **545**, 185-203) and Ase1-GFP[11] were grown as described previously (Tran, P.T. et al. 2004 *Methods* **33**, 220-225). Imaging was performed by spinning disk confocal microscopy as described for the FRAP imaging above. mRFP and GFP images were obtained sequentially at a frame rate of 1 frame per 3 seconds.

Table S1 Parameters of the model.

Model parameter		Unit
Overlap length	L	µm
Number of Ase1 in the overlap	n	AU
Ase1 density in the overlap	ρ	AU µm^{-1}
Sliding velocity	v	nm s^{-1}
Sweeping efficiency	ε	-
Ase1 on rate	k_{on}	AU µm^{-1} s^{-1}
Ase1 off rate	k_{off}	s^{-1}

Supplementary Movie Legends

Movie S1 Ase1-GFP brakes Ncd-driven MT-MT sliding. Progressive slowdown of a transport MT (bright red) sliding on a template MT (dim red) after the addition of Ase1-GFP (green). Same data as in Figs. 1b and 1c. Ase1-GFP is flushed at 1.2 minutes after binding of the shown transport MT, corresponding to about 2 minutes in the time code of the movie. Time given in minutes:seconds. This movie corresponds to Figs. 1b and 1c.

Movie S2 Ase1-GFP prevents MTs from sliding apart completely. Ase1-GFP (green) prevents overlapping MTs (red) from sliding apart. Time given in minutes:seconds. This movie corresponds to Fig. 2a.

Movie S3 Single Ase1-GFP molecules in MT-MT overlap. Timelapse movie showing transient interactions of individual Ase1-GFP dimers with a single MT. This movie corresponds to Fig. S4.

Movie S4 Measurement and model of Ase1-GFP adaptive braking of MT sliding. Timelapse movies and kymographs showing the formation of stable MT overlaps between template MT (dim red) and transport MT (bright red) in the presence of Ase1-GFP (green). Experimental data (left) and simulation (right) correspond to the kymograph in Fig. 4c. Artificial microscopy images were created to visualize the model calculations. We calculated the number of fluorophores for both MTs consistent with our experimental labeling ratios (1:20 for template MT and 1:3 for transport MT). Next, fluorophores were randomly placed on the surface of a MT and we modeled their point-spread-functions by symmetric two-dimensional Gaussians (FWHM=600 nm). The intensity of each fluorophore was determined using a Poisson distribution of given mean value λ. Poisson noise (to simulate photon shot noise) and Gaussian noise (to simulate dark noise of the camera) were added to every pixel. Ase1-GFP signals were simulated based on randomly positioned molecules in the MT ovelap (100 molecules at the start of the simulation). The length of the MT overlap and the temporal evolution of the number of Ase1-GFP molecules were calculated according to the model. Bleaching was not taken into account. This movie corresponds to Fig. 4c.

Movie S5 Ase1-GFP sweeping in live S. pombe cells. Timelapse movie showing MT dynamics in a *S. pombe* cell during interphase. This movie corresponds to Fig. S6.